



Influence of operation conditions on the performance of pilot-scale vacuum membrane distillation (VMD)

Yonghyun Shin, Jihyuk Choi, Youngkyu Park, Yongjun Choi, Sangho Lee*

School of Civil and Environmental Engineering, Kookmin University, Jeongneung-Dong, Seongbuk-Gu, Seoul 136-702, Korea, Tel. +82-2-910-4529; Fax: +82-2-910-4939; email: sanghlee@kookmin.ac.kr (S. Lee)

Received 6 October 2016; Accepted 21 November 2016

ABSTRACT

Although many studies have been done on membrane distillation (MD) for seawater desalination and wastewater treatment, relatively few works have been done in pilot- or full-scale plants. Accordingly, this study intended to investigate the performance of a vacuum MD system at pilot scale. Factors affecting MD flux were examined, including feed temperature, feed flow rate, and applied vacuum. Results showed that the MD flux was almost linearly proportional to feed temperature and flow rate. Moreover, the flux was also sensitive to the applied vacuum. Based on the analysis, the minimum feed temperature and vacuum to operate the MD pilot plant were determined to be 56°C and 0.28 bar, respectively. The flux and energy utilization ratio were analyzed as a function of feed temperature and flow rate, indicating that the feed temperature should be over 69°C to obtain flux over 4 kg/m² h and the feed flow rate should be over 5.6 m³/h to achieve energy utilization ratio above 0.65.

Keywords: Membrane distillation; Flux; Energy utilization ratio; Pilot plant; Operation conditions

1. Introduction

With increasing stress on freshwater resources, the use of seawater desalination has rapidly grown for countries in coastal areas [1–3]. Seawater desalination offers a sustainable way to provide freshwater supply without relying on climate conditions and rainfall patterns [4–6]. It can be also considered as an effective method in emergency situations such as severe drought and accidental surface/ground water contamination [2,7–9]. This is why the desalination market is growing not only in Middle East regions but also in other coastal regions [1,2].

Nevertheless, seawater desalination technologies such as reverse osmosis, multi-stage flash, and multi-effect distillation have problems related to their high energy consumption [3,5]. Moreover, these technologies are based on the energy from the fossil fuels, resulting in the production of greenhouse gases [3,4,6]. Accordingly, there is a need to develop desalination technologies that can reduce the consumption of

energy from fossil fuels [10–15]. Among various techniques, of particular interest is membrane distillation (MD) that can use thermal energy for desalination [14,16,17]. MD uses hydrophobic porous membranes to separate saline water from water vapor, which allows the removal of salts from the feedwater [17,18]. The difference in the temperature between the feed and distillate, which is the driving force for MD, can be obtained using solar thermal energy or water heat from industrial plants [18,19]. Therefore, there are possibilities that MD can be more sustainable than other desalination technologies with increased use of renewable energy sources [20,21].

There are four representative configurations for MD modules [17,18]: direct contact membrane distillation (DCMD), air gap membrane distillation (AGMD), vacuum membrane distillation (VMD), and sweeping gas membrane distillation. Compared with DCMD, AGMD and VMD have higher thermal energy efficiency due to the reduction in conductive heat loss through the membrane. However, the water flux in AGMD is relatively lower than those in DCMD and VMD due to the existence of the air gap acting as additional mass transfer resistance. In case of flat sheet membranes, all four

* Corresponding author.

types of MD modules can be considered. However, in case of hollow fiber membranes, only DCMD and VMD can be primarily considered due to their inherent restriction. Although a few attempts were made to use hollow fiber membranes for AGMD, they are quite complicated and difficult to use in practical applications.

Since 1963, there have been a lot of works on MD for the development of membrane materials, modules, processes, theoretical models, and so on [16–34]. On the other hand, relatively few studies focused on pilot- or full-scale implementations of MD, which are essential for practical applications in industry. Therefore, the primary objective of this study was to investigate MD in a pilot scale to understand the effect of operation conditions on its performance such as flux and energy utilization ratio. Hollow fiber membranes in VMD module were used in a pilot plant with the maximum water production capacity of 10 m³/d. The effect of feed temperature, feed flow rate, and applied vacuum were considered as the major operation parameters.

2. Experimental

2.1. The VMD pilot plant

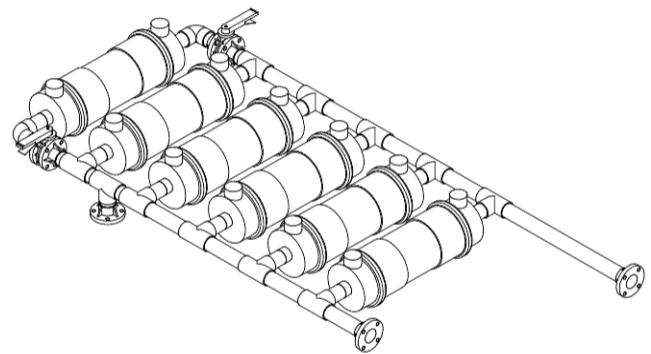
The VMD pilot plant was built in a project named Global MVP supported by Ministry of Land, Infrastructure and Transport of Korean government. The schematic diagram of the pilot plant is shown in Fig. 1. The plant consists of five modules arranged in the first stage and the 10 modules arranged in the second stage. It could be operated either in single stage or two stage modes. In the full load condition, the pilot plant could produce water up to 10 m³/d. The module was connected in parallel as shown in Fig. 2. The MD modules are assembled and supplied by Econity, Korea. The active membrane area for each module is 7.6 m². The modules contain hollow fiber membranes made of polyvinylidene fluoride. The membrane characteristics are 0.2 mm thickness (ID: 0.8 mm, OD: 1.2 mm), 0.1 μm average pore size, and 80% porosity. The size of one module is 45 cm long and a shell diameter of 16.3 cm. The details on the MD module are summarized in Table 1.

2.2. Experimental procedures

A series of MD experiments were performed by adjusting operation conditions. The feed flow rates were controlled from 1 to 7.2 m³/h. The feed inlet temperature was regulated from 56°C to 75°C and the vacuum was ranged from 0.15 to 0.24 bar. The feedwater was the surface water with the TDS of 250 mg/L.



(a)



(b)

Fig. 2. MD module array (a) photograph and (b) 3D model.

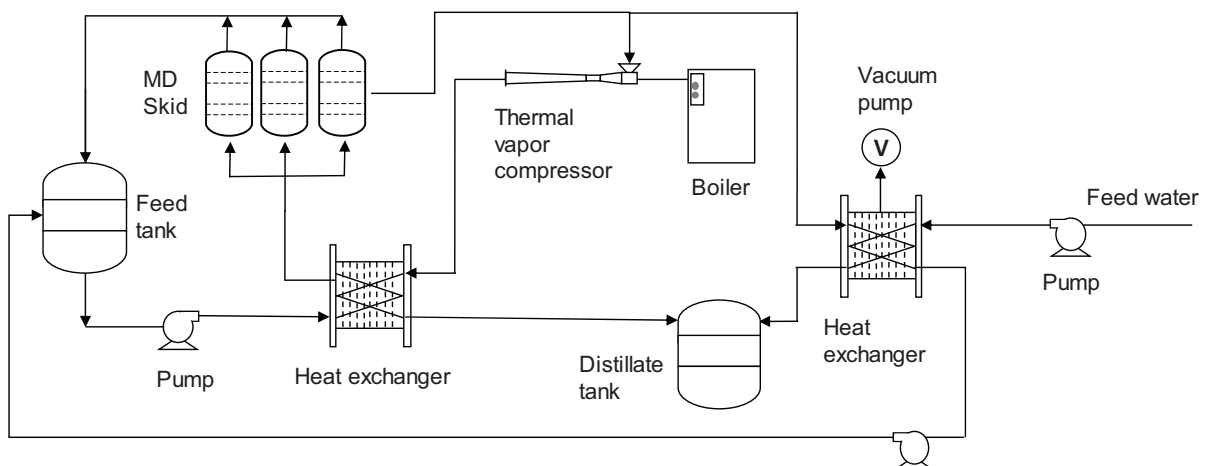


Fig. 1. Schematic diagram for vacuum membrane distillation (VMD) pilot plant.

Table 1
Properties of MD membrane module

| Parameters | Values |
|--------------------------|------------------------|
| Shell diameter | 0.163 m |
| Fiber inside diameter | 0.8×10^{-3} m |
| Fiber outside diameter | 1.2×10^{-3} m |
| Average pore size | 0.1×10^{-6} m |
| Porosity | 0.8 |
| Module length | 0.45 m |
| Membrane area per module | 7.6 m ² |

During the experiments, all experimental data were recorded using the equipments connected to the control system. Temperature sensors were installed close to the MD module's inlet and outlet streams to monitor feed and brine temperatures. A conductivity analyzer was used to check the conductivity of the product water, which confirmed the 99.9% of ion rejection under all conditions in this study. Online flow meters were used to measure feed flow rates and product water flux.

3. Results and discussion

3.1. Effect of feed temperature

Fig. 3 shows the variation in product water flux with feed temperature during the MD operation. The flux increases with increasing feed temperatures since the driving force for MD increases with an increase in the feed temperature. As a matter of fact, a linear relationship between the feed temperature and flux was observed with the maximum flux of 6.76 kg/m² h at 74.2°C. On the other hand, the flux decreased to zero as the feed temperature was reduced lower than 56°C. Based on these results, it is recommended that the feed temperature should be at least higher than 56°C.

The minimum feed temperature required for VMD operation is related to the degree of applied vacuum. Since the VMD needs the net difference in vapor pressure between feed and distillate side, the vapor pressure in the feed side should be higher than the applied vacuum. The vapor pressure is calculated using the Antoine equation [18,29]:

$$p_w = \exp\left(a_1 - \frac{a_2}{T_m + a_3}\right) \quad (1)$$

$$\frac{p_w}{p_s} = 1 + 0.57357\left(\frac{S}{1000 - S}\right) \quad (2)$$

where p_w is the vapor pressure for pure water; p_s is the vapor pressure for saline water; a_1 , a_2 , and a_3 are the Antoine parameters, which are 23.238, 3882.89, and -42.85 K, respectively, for pure water; and S is the salinity expressed in g/kg. According to these equations, the feed temperature required to have the vapor pressure of 0.15 bar is 54°C. This is why the minimum temperature for VMD was 0.56°C, which is slightly higher than the theoretical minimum.

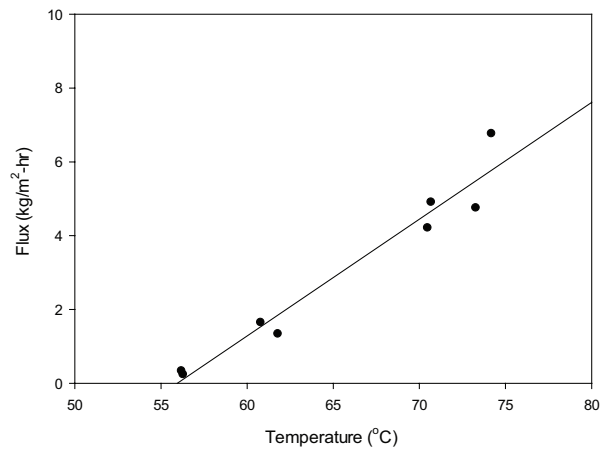


Fig. 3. Effect of feed temperature on MD flux (operation conditions: feed flow rate 6 m³/h and applied vacuum 0.15 bar).

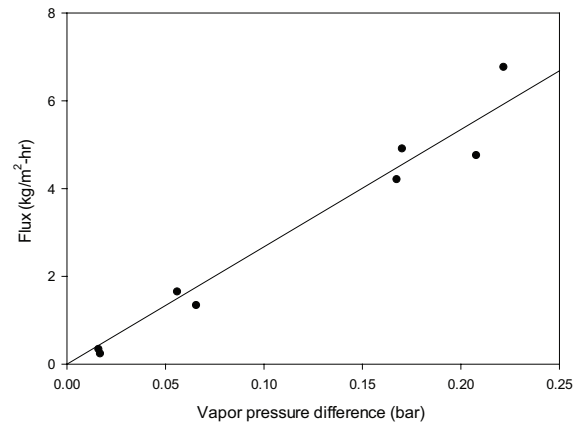


Fig. 4. Effect of feed temperature on MD flux (operation conditions: feed flow rate 6 m³/h and applied vacuum 0.15 bar).

In Fig. 4, the flux was shown as a function of the pressure difference between the feed side and the distillate side (vacuum side). The vapor pressure for the feedwater was calculated using Eqs. (2) and (3). As expected, there is a linear relationship between the vapor pressure difference and flux.

3.2. Effect of feed flow rate

Together with the feed temperature, the feed flow rate is also one of the main operation parameters affecting the performance of MD. Fig. 5 shows how the feed flow rate changes the flux. As the feed flow rate increased, the flux increased due to the combined effects of high shear rate and increased thermal energy supply: first, the increase in the feed flow rate results in a reduction in concentration polarization as well as temperature polarization, leading to an increase in the flux. In addition, the total thermal energy (sensible heat) supplied to the MD module increases with increasing the feed flow rate, thereby increasing the flux. In fact, the flow rate <3 m³/h resulted in much lower flux (~2 kg/m² h) than the other flow rates. It appears that the feed flow rate should be >3 m³/h per module or 0.395 m³/h per m² of the membrane area.

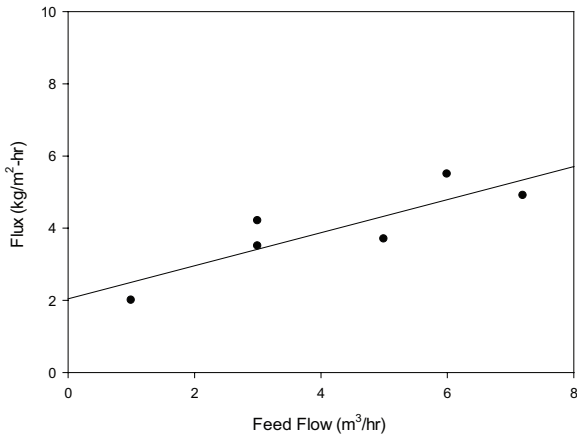


Fig. 5. Effect of feed flow rate on MD flux (operation conditions: feed temperature 70°C and applied vacuum 0.15 bar).

3.3. Effect of applied vacuum

As mentioned above, the vacuum pressure is important in determining the flux because the driving force for VMD is the pressure difference between the feed vapor pressure and the vacuum pressure. As shown in Fig. 6, the flux decreases from 5.97 to 1.95 kg/m² h with increasing the vacuum pressure from 0.15 to 0.24 bar. If the vacuum pressure is set to 0.24 bar, the minimum feed temperature should be raised up to 64.5°C.

3.4. Effect of thermal energy supply

The amount of thermal energy supplied to an MD module is calculated from the difference in thermal energy between the feed and brine [18,29]:

$$Q_{in} = \rho q_{f,in} C_p T_{f,in} - \rho q_{f,out} C_p T_{f,out} \quad (3)$$

where ρ is the water density, $q_{f,in}$ is the feed inflow rate, $q_{f,out}$ is the feed outflow rate, C_p is the heat capacity of water, $T_{f,in}$ is the feed inlet temperature, and $T_{f,out}$ is the feed outlet temperature. On the other hand, the thermal energy used for water production is given by [18,29]:

$$Q_{flux} = J_w H_w A_m = \eta Q_{in} \quad (4)$$

where H_w is the latent heat of water vaporization, A_m is the membrane area, J_w is the distillate flux, and η is the thermal energy utilization ratio. Accordingly, it is expected that the flux increases with an increase in the thermal energy supply. As shown in Fig. 7, a linear relationship between the thermal energy supply and the flux was obtained based on the analysis using the experimental results.

3.5. Flux and energy utilization ratio

In addition to the experiments shown above, a series of experiments were carried out to reveal the effect of operation conditions such as feed flow rate and feed temperature on flux and energy utilization ratio (η). Fig. 8(a) shows the

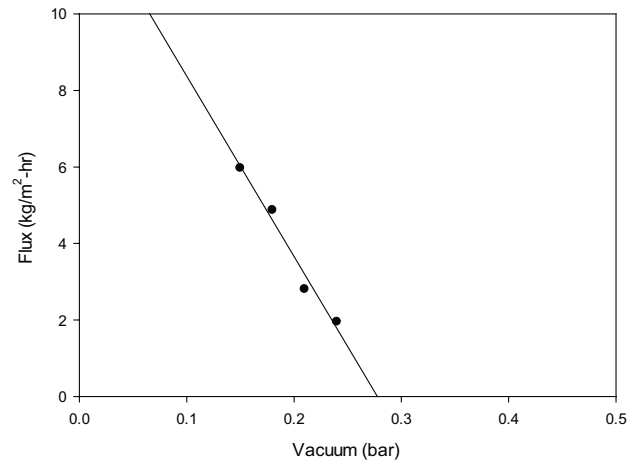


Fig. 6. Effect of applied vacuum on MD flux (operation conditions: feed flow rate 6 m³/h and feed temperature 70°C).

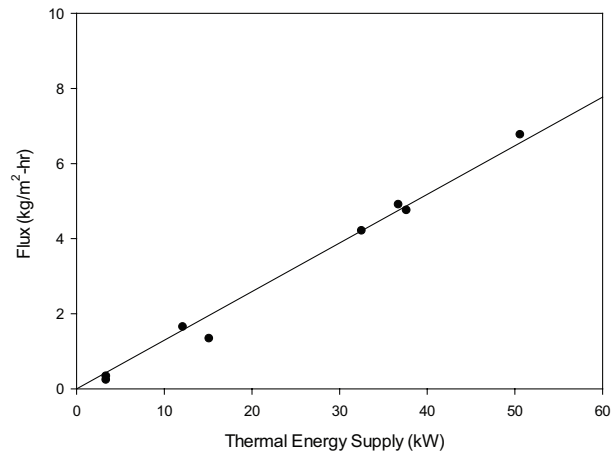


Fig. 7. Correlation between thermal energy supply and MD flux.

contour for the flux under various operation conditions on the flux. As the feed flow rate and feed temperature increase, the flux increases as expected. However, it seems that the flux is more sensitive to the feed temperature on the feed flow rate. For example, the feed temperature should be higher than 69°C to obtain the flux higher than 4 kg/m² h. Below this temperature, it is not possible to achieve this condition by simply increasing the flow rate.

As the feedwater passes through the MD module, a portion of thermal energy is used to evaporate water and the brine temperature decreases. Fig. 8(b) shows the contour for the temperature drop in feed side as a function of the feed flow rate and the temperature. In this case, both the feed temperature and the feed flow rate are important. As the feed flow rate increases and the feed temperature decreases, the temperature drop decreases. The maximum temperature drop was 7°C.

Fig. 9(a) shows the contour for the temperature difference between the feed and vapor from the MD module. In an ideal case, the vapor temperature should be identical to the average temperature of the feed stream in the MD module. However, due to thermal energy losses and temperature polarization,

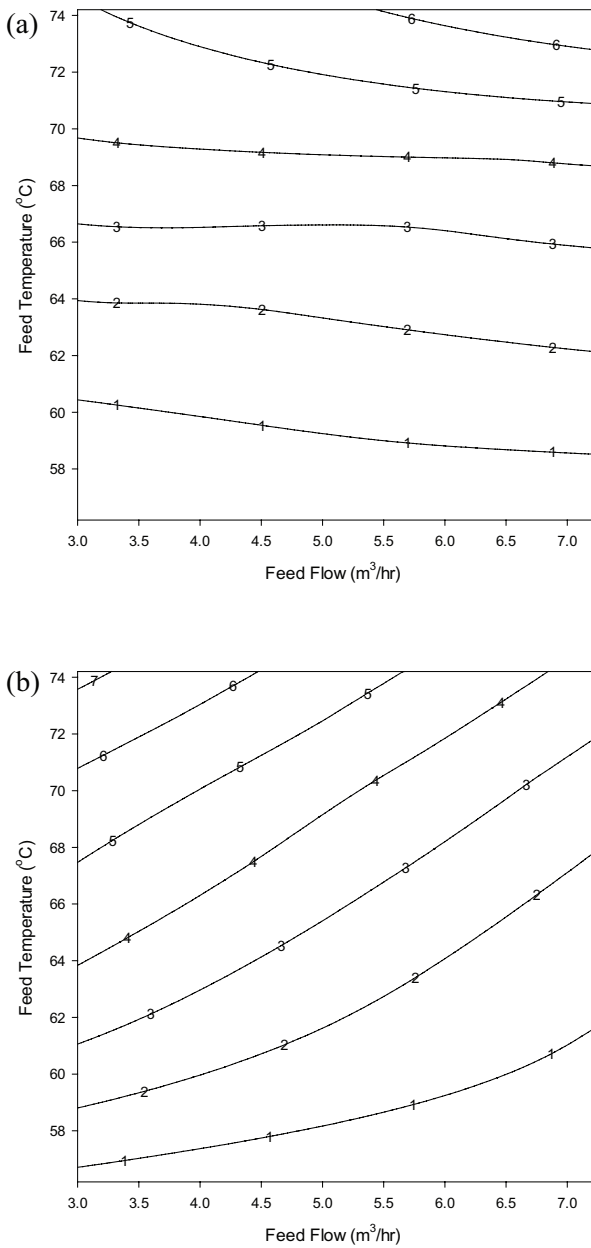


Fig. 8. Contours of flux and temperature drop in the MD brine as a function of feed flow rate and feed temperature (a) flux and (b) temperature difference between feed and brine.

it is lower than the feed temperature. As the feed flow temperature increases and the feed flow rate decreases, the temperature difference increases. Unlike the feed temperature drop, however, the temperature drop between the feed and vapor was more highly dependent on the feed temperature than the feed flow rate. The maximum temperature difference was 14.7°C.

Finally, the thermal energy utilization ratio (η) was estimated using Eq. (4) and shown as a function of the feed temperature and feed flow rate as illustrated in Fig. 9(b). In general, η increases with an increase in the feed flow rate

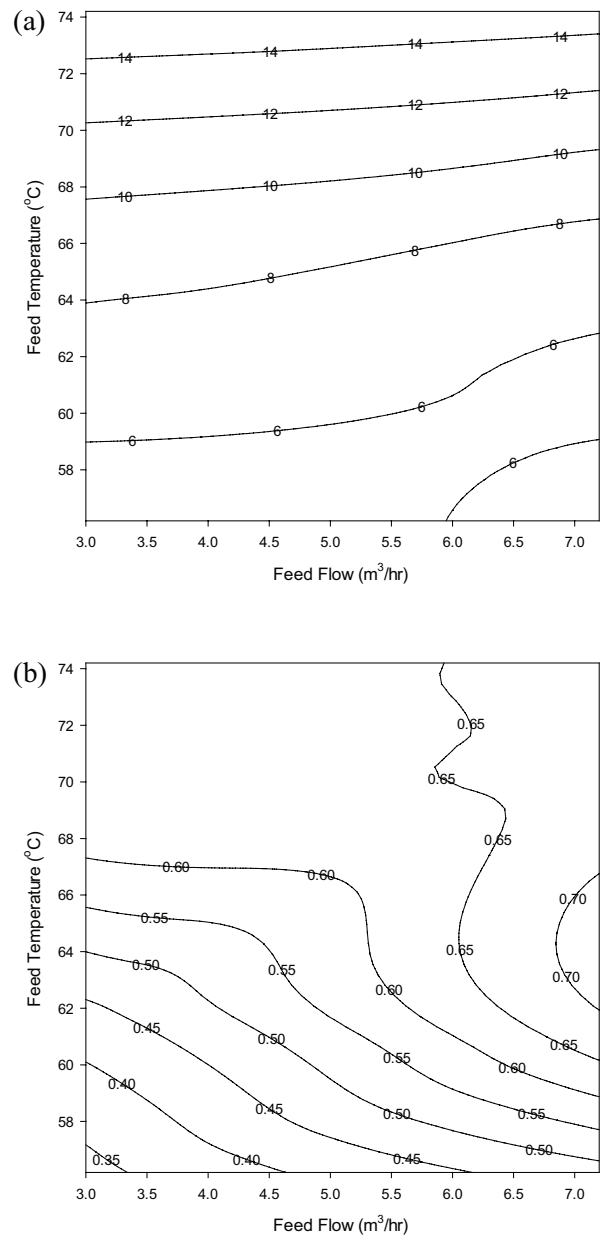


Fig. 9. Contours of temperature drop in the MD steam and thermal energy utilization as a function of feed flow rate and feed temperature (a) temperature difference between feed and distillate and (b) thermal energy utilization ratio.

and the temperature. However, it shows a maximum value at the feed flow rate of 7.2 m³/h and the feed temperature of 64°C. Moreover, the feed flow rate should be over 5.6 m³/h to achieve energy utilization ratio above 0.65. This suggests that the thermal energy efficiency for the MD module is the highest under this condition. Of course, it does not imply the total energy efficiency for the MD plant because the energy in the vapor is recovered by the TVC and heat exchanger. Nevertheless, it still implies that the changing pattern of η does not match that of the flux. The flux showed its maximum at the highest feed temperature and flow rate. On the

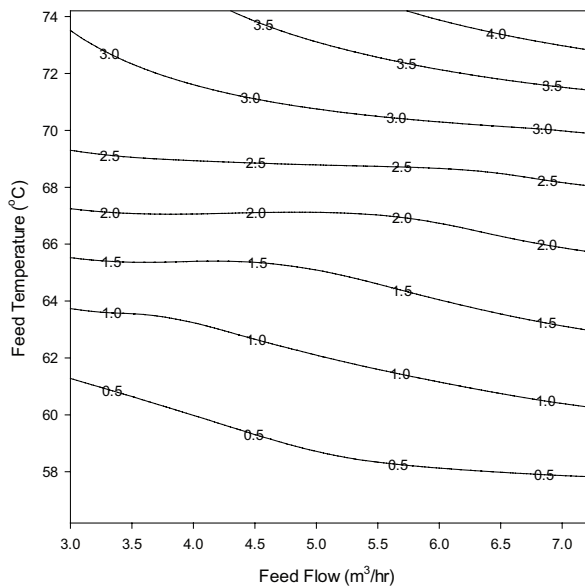


Fig. 10. Contours of performance index as a function of feed flow rate and feed temperature.

other hand, η showed its maximum at an intermediate temperature. This may be attributed to the difference in the thermal energy loss under different operation conditions.

3.6. Performance index

Since the flux and η are both important in MD operation, it is necessary to consider two factors simultaneously. Accordingly, the performance index, which is defined as the product of flux and η , is suggested to compare the efficiency of MD operation under different conditions. Fig. 10 shows the contour for the performance index as a function of the feed flow rate and the feed temperature. As expected, an increase in the feed temperature and the feed flow rate results in an increase in the performance ratio. This can be used to explore the operation conditions to satisfy a given condition. For example, if the performance index should be higher than 2.0, the combinations of the feed flow rate and the feed temperature can be found from this contour. The feed temperature should be higher than 67.5°C at 3.0 m³/h and 66°C at 7.2 m³/h.

4. Conclusion

In this study, the performance of a VMD was investigated in a pilot plant under various feed temperatures, feed flow rates, and applied vacuums. The following conclusions were drawn:

- The flux was linearly proportional to the feed temperature within the conditions considered in this study. The minimum feed temperature, which was 56°C in our pilot plant, was determined by the degree of the applied vacuum.
- The feed flow rate was found to be also an important factor affecting the flux. Below the flow rate of 3 or 0.395 m³/h per m² of the membrane area, the flux significantly

decreased. As the applied vacuum pressure increased, the flux decreased. The minimum vacuum pressure at the feed temperature of 70°C was 0.27 bar.

- Contours for flux and thermal energy utilization ratio (η) were constructed as a function of the feed temperature and feed flow rate. The flux increased with increasing the temperature and the flow rate. However, η showed the maximum value at high flow rate and an intermediate temperature (~64°C). Based on these results, the performance index defined as the product of the flux and η was suggested.

Acknowledgment

This research was supported by a grant (code 16IFIP-B065893-04) from Industrial Facilities & Infrastructure Research Program funded by Ministry of Land, Infrastructure and Transport of Korean government.

References

- [1] X. Zheng, D. Chen, Q. Wang, Z. Zhang, Seawater desalination in China: retrospect and prospect, *Chem. Eng. J.*, 242 (2014) 404–413.
- [2] J.R. Ziolkowska, R. Reyes, Prospects for Desalination in the United States—Experiences From California, Florida, and Texas, Chapter 3.1.3, *Competition for Water Resources*, Elsevier, 2017, pp. 298–316.
- [3] G. Amy, N. Ghaffour, Z. Li, L. Francis, R.V. Linares, T. Missimer, S. Lattemann, Membrane-based seawater desalination: present and future prospects, *Desalination*, 401 (2017) 16–21.
- [4] T.-K. Liu, H.-Y. Sheu, C.-N. Tseng, Environmental impact assessment of seawater desalination plant under the framework of integrated coastal management, *Desalination*, 326 (2013) 10–18.
- [5] M.P. Shahabi, A. McHugh, M. Anda, G. Ho, Comparative economic and environmental assessments of centralised and decentralised seawater desalination options, *Desalination*, 376 (2015) 25–34.
- [6] V. Martínez-Alvarez, B. Martín-Gorri, M. Soto-García, Seawater desalination for crop irrigation — a review of current experiences and revealed key issues, *Desalination*, 381 (2016) 58–70.
- [7] N. Heck, A. Paytan, D.C. Potts, B. Haddad, Predictors of local support for a seawater desalination plant in a small coastal community, *Environ. Sci. Policy*, 66 (2016) 101–111.
- [8] J. Liu, S. Chen, H. Wang, X. Chen, Calculation of carbon footprints for water diversion and desalination projects, *Energy Procedia*, 75 (2015) 2483–2494.
- [9] A. Turner, O. Sahin, D. Giurco, R. Stewart, M. Porter, The potential role of desalination in managing flood risks from dam overflows: the case of Sydney, Australia, *J. Cleaner Prod.*, 135 (2016) 342–355.
- [10] J. Imbrogno, J.J. Keating IV, J. Kilduff, G. Belfort, Critical aspects of RO desalination: a combination strategy, *Desalination*, 401 (2017) 68–87.
- [11] Q. Chen, Y. Li, K.J. Chua, On the thermodynamic analysis of a novel low-grade heat driven desalination system, *Energy Convers. Manage.*, 128 (2016) 145–159.
- [12] A. Christ, B. Rahimi, K. Regenauer-Lieb, H.T. Chua, Techno-economic analysis of geothermal desalination using hot sedimentary aquifers: a pre-feasibility study for Western Australia, *Desalination*, 404 (2017) 167–181.
- [13] N. Ghaffour, J. Bundschuh, H. Mahmoudi, M.F.A. Goosen, Renewable energy-driven desalination technologies: a comprehensive review on challenges and potential applications of integrated systems, *Desalination*, 356 (2015) 94–114.
- [14] A. Subramani, J.G. Jacangelo, Emerging desalination technologies for water treatment: a critical review, *Water Res.*, 75 (2015) 164–187.

- [15] D. Zhao, S. Chen, C.X. Guo, Q. Zhao, X. Lu, Multi-functional forward osmosis draw solutes for seawater desalination, *Chin. J. Chem. Eng.*, 24 (2016) 23–30.
- [16] A.M. Karam, A.S. Alsaadi, N. Ghaffour, T.M. Laleg-Kirati, Analysis of direct contact membrane distillation based on a lumped-parameter dynamic predictive model, *Desalination*, 402 (2017) 50–61.
- [17] M.A.E.-R. Abu-Zeid, Y. Zhang, H. Dong, L. Zhang, H.-L. Chen, L. Hou, A comprehensive review of vacuum membrane distillation technique, *Desalination*, 356 (2015) 1–14.
- [18] I. Hitsov, T. Maere, K. De Sitter, C. Dotremont, I. Nopens, Modelling approaches in membrane distillation: a critical review, *Sep. Purif. Technol.*, 142 (2015) 48–64.
- [19] L.D. Tijing, Y.C. Woo, J.-S. Choi, S. Lee, S.-H. Kim, H.K. Shon, Fouling and its control in membrane distillation—a review, *J. Membr. Sci.*, 475 (2015) 215–244.
- [20] B.B. Ashoor, S. Mansour, A. Giwa, V. Dufour, S.W. Hasan, Principles and applications of direct contact membrane distillation (DCMD): a comprehensive review, *Desalination*, 398 (2016) 222–246.
- [21] Y. Zhang, Y. Peng, S. Ji, Z. Li, P. Chen, Review of thermal efficiency and heat recycling in membrane distillation processes, *Desalination*, 367 (2015) 223–239.
- [22] J. Deshpande, K. Nithyanandam, R. Pitchumani, Analysis and design of direct contact membrane distillation, *J. Membr. Sci.*, 523 (2017) 301–316.
- [23] D.M. Warsinger, J. Swaminathan, E. Guillen-Burrieza, H.A. Arafat, J.H. Lienhard V, Scaling and fouling in membrane distillation for desalination applications: a review, *Desalination*, 356 (2015) 294–313.
- [24] A. Khalifa, H. Ahmad, M. Antar, T. Laoui, M. Khayet, Experimental and theoretical investigations on water desalination using direct contact membrane distillation, *Desalination*, 404 (2017) 22–34.
- [25] E.-J. Lee, A.K. An, T. He, Y.C. Woo, H.K. Shon, Electrospun nanofiber membranes incorporating fluorosilane-coated TiO₂ nanocomposite for direct contact membrane distillation, *J. Membr. Sci.*, 520 (2016) 145–154.
- [26] L. Li, K.K. Sirkar, Studies in vacuum membrane distillation with flat membranes, *J. Membr. Sci.*, 523 (2017) 225–234.
- [27] G. Naidu, W.G. Shim, S. Jeong, Y. Choi, N. Ghaffour, S. Vigneswaran, Transport phenomena and fouling in vacuum enhanced direct contact membrane distillation: experimental and modelling, *Sep. Purif. Technol.*, 172 (2017) 285–295.
- [28] L.-F. Ren, F. Xia, J. Shao, X. Zhang, J. Li, Experimental investigation of the effect of electrospinning parameters on properties of superhydrophobic PDMS/PMMA membrane and its application in membrane distillation, *Desalination*, 404 (2017) 155–166.
- [29] D. Woldemariam, A. Kullab, U. Fortkamp, J. Magner, H. Royen, A. Martin, Membrane distillation pilot plant trials with pharmaceutical residues and energy demand analysis, *Chem. Eng. J.*, 306 (2016) 471–483.
- [30] Y.C. Woo, L.D. Tijing, W.-G. Shim, J.-S. Choi, S.-H. Kim, T. He, E. Drioli, H.K. Shon, Water desalination using graphene-enhanced electrospun nanofiber membrane via air gap membrane distillation, *J. Membr. Sci.*, 520 (2016) 99–110.
- [31] H. Zhang, M. Liu, D. Sun, B. Li, P. Li, Evaluation of commercial PTFE membranes for desalination of brine water through vacuum membrane distillation, *Chem. Eng. Process.*, 110 (2016) 52–63.
- [32] J. Zuo, T.-S. Chung, G.S. O'Brien, W. Kosar, Hydrophobic/hydrophilic PVDF/Ultem® dual-layer hollow fiber membranes with enhanced mechanical properties for vacuum membrane distillation, *J. Membr. Sci.*, 523 (2017) 103–110.
- [33] A. Ali, C.A. Quist-Jensen, F. Macedonio, E. Drioli, Optimization of module length for continuous direct contact membrane distillation process, *Chem. Eng. Process.*, 110 (2016) 188–200.
- [34] H. Julian, S. Meng, H. Li, Y. Ye, V. Chen, Effect of operation parameters on the mass transfer and fouling in submerged vacuum membrane distillation crystallization (VMDC) for inland brine water treatment, *J. Membr. Sci.*, 520 (2016) 679–692.